An extended FGM model with transported PDF for LES of spray combustion

Hadadpour, Ahmad; Xu, Shijie; Zhang, Yan; Bai, Xue Song; Jangi, Mehdi

DOI:
10.1016/j.proci.2022.09.014

Available online at www.sciencedirect.com
ScienceDirect
Proceedings of the Combustion Institute 000 (2022) 1–10
Proceedings of the Combustion Institute
www.elsevier.com/locate/proci

An extended FGM model with transported PDF for LES of spray combustion

Ahmad Hadadpour [a,b,*], Shijie Xu [a,*], Yan Zhang [a,c], Xue-Song Bai [a], Mehdi Jangi [d]

[a] *Division of Fluid Mechanics, Department of Energy Science, Lund University, P.O. Box 118, 221 00 Lund, Sweden*
[b] *Scania CV AB, SE-15187 Södertälje, Sweden*
[c] *State Key Laboratory of Engines, Tianjin University, 300350 Tianjin, P.R. China*
[d] *Department Mechanical Engineering, School of Engineering, University of Birmingham, B15 2TT Birmingham, UK*

Received 4 January 2022; accepted 2 September 2022
Available online xxx

Abstract

An enhanced flamelet generated manifold (FGM) model for large eddy simulation (LES) of turbulent spray combustion is presented. In the enhanced FGM model, a transported probability density function (TPDF) description of the FGM variables is employed. The TPDF is represented using the Eulerian stochastic fields (ESF) approach, and the method is applied to LES of spray combustion under conditions relevant to internal combustion engines. The new ESF/FGM method achieves an improved accuracy of predictions due to the ESF modelling of the subgrid-scale turbulence-chemistry interaction. It also achieves high computational efficiency due to the FGM tabulation of the chemical kinetic mechanism. The performance of the new ESF/FGM model is assessed by simulation of the Spray-A flames from Engine Combustion Network (ECN) and comparison of the results, firstly, with experimental measurements, and secondly, with conventional FGM model simulation results. It is shown that the ESF/FGM method is capable of predicting both global and local combustion characteristics, i.e., pressure rise, ignition delay time, flame lift-off length and the thermo-chemical structure of the spray flames with improved accuracy compared to the conventional FGM model that is based on the presumed PDF description of FGM variables. The sensitivity of the predictions using ESF/FGM to the number of stochastic fields is examined by varying the number of these fields in the range of 4–128. Furthermore, the influence of different FGM reaction progress variables on the simulations is investigated, and a new reaction progress variable based on the local consumption of oxygen is proposed. The results show that the new progress variable improves predictions of spray combustion, including the prediction of the start of injection, the quasi-steady state liftoff length, the post-injection oxidation, and the pressure evolution.

Keywords: LES; Spray combustion; Flamelet generated manifold (FGM); Eulerian stochastic fields (ESF); Reaction progress variable; Engine combustion network (ECN)

* Corresponding author.
E-mail addresses: ahmad.hadadpour@scania.com (A. Hadadpour), shijie.xu@energy.lth.se (S. Xu).

https://doi.org/10.1016/j.proci.2022.09.014

1. Introduction

Spray combustion in modern internal combustion engines is a two-phase, multi-physics and multi-scale phenomenon [1]. It occurs in a confined high-pressure and high-temperature environment that is hardly accessible for detailed experimental diagnostics. Numerical simulations of spray combustion, therefore, enable engine researchers to cope with the experimental limitations.

One of the most widely used modelling concepts for the numerical simulations of combustion is the flamelet concept. This includes, among others, the flamelet progress variable method (FPV) [2], the unsteady flamelet progress variable method (UFPV) [3] and the flamelet generated manifold method (FGM) [4]. Typically, the methods in the framework of the flamelet concept rely on the following three general assumptions: (a) The thermodynamic state of each point in the computational domain can be described by a few principal variables, e.g., the mixture fraction (Z) and the reaction progress variable ($\mathcal{Y}$). (b) The probability density function (PDF) of these principle variables, which are needed to calculate the mean thermodynamic variables, are assumed to be statistically independent. (c) The statistical distributions of these variables follow a prescribed PDF function. These assumptions introduce a great simplicity to the problem and allow computationally efficient modelling of spray flames. The results are also accurate for the conditions that the aforementioned assumptions are valid. However, combustion in modern engines may not satisfy all the flamelet assumptions; hence, the accuracy of the simulation results of the model may be poor.

The transported PDF (TPDF) with finite rate chemistry is a more sophisticated turbulent combustion modelling approach. This approach does not rely on the aforementioned assumptions, since the turbulence/chemistry interaction (TCI) in TPDF is taken into account using transport equations of the PDF. In particular, in the context of large eddy simulation (LES) using TPDF approach, the filtered reaction source terms in the species transport equations appear in a closed form, which eliminates the need for further assumptions on the modelling of highly non-linear reaction rates [5,6]. The major drawback of the TPDF approach with finite rate chemistry is its high computational costs, which makes it less attractive for modelling of engineering combustion processes.

Here, we investigate a new concept by coupling the TPDF concept with the FGM concept. The idea of coupling TPDF with FGM was first tested for simulation of non-premixed bluff-body stabilized CH_4/H_2 flame [7], stratified lean premixed flame [8] and non-premixed oxyfuel flame [9]. In this work, the concept is extended and applied to multi-phase spray combustion with autoignition. The method benefits from the computational efficiency of FGM and the accuracy of TPDF. The main idea is to use TPDF to relax the major assumptions on the PDF of FGM variables. More specifically, the aforementioned assumptions (b) and (c) in the presumed-PDF flamelet approach are eliminated, and the joint-PDF of FGM variables is represented using TPDF equations. The TPDF equations are solved using the Eulerian stochastic fields (ESF) approach [5,10], and the new approach is hereafter referred to as ESF/FGM.

2. Numerical method

2.1. Large eddy simulation of the spray flame

The Favre-filtered conservation equations for mass and momentum for turbulent spray flames are:

$$\frac{\partial \overline{\rho}}{\partial t} + \frac{\partial \overline{\rho}\tilde{u}_j}{\partial x_j} = \overline{S_\rho^s}, \tag{1}$$

$$\frac{\partial \overline{\rho}\tilde{u}_i}{\partial t} + \frac{\partial}{\partial x_j}(\overline{\rho}\tilde{u}_i\tilde{u}_j - \overline{\tau}_{ij} - \tau_{ij}^{sgs}) = \overline{S_{u_i}^s}. \tag{2}$$

Here, the overline denotes the spatial filtering and the tilde denotes the Favre filtering; u_i is velocity component along x_i-direction; ρ is density; $\overline{\tau}_{ij}$ is filtered viscous stress tensor obtained from the resolved strained rate. τ_{ij}^{sgs} is the subgrid-scale (SGS) term modeled using one-equation eddy-viscosity approach. The terms with superscript s are spray source terms, which account for the liquid-gas exchange rate of the mass ($\overline{S_\rho^s}$) and momentum ($\overline{S_{u_i}^s}$). The closure for these terms is obtained using the Lagrangian particle tracking (LPT) method.

2.2. Turbulent combustion modelling

In FGM modelling of turbulent spray combustion, the thermochemical properties (hereinafter referred to as ψ_α, e.g., species mass fraction Y_i and the reaction source terms) are calculated from the FGM tables. The entry quantities for these tables are Z and $\mathcal{C}$, i.e., $F_{\psi_\alpha}(Z,\mathcal{C})$, where $\mathcal{C}$ is normalized $\mathcal{Y}$, $\mathcal{C} = (\mathcal{Y} - \mathcal{Y}_{\min}(Z))/(\mathcal{Y}_{\max}(Z) - \mathcal{Y}_{\min}(Z))$. The joint-PDF of Z and $\mathcal{C}$ in the subgrid scales for each computational cell, $\tilde{P}(Z,\mathcal{C})$, is required to take the TCI into account. Thus, the filtered terms ($\tilde{\psi}_\alpha$) can be calculated as:

$$\tilde{\psi}_\alpha = \iint F_{\psi_\alpha}(Z,\mathcal{C})\tilde{P}(Z,\mathcal{C})dZd\mathcal{C}. \tag{3}$$

The first main contribution of the current work is to improve the representation of such joint-PDF for spray combustion simulations.

2.2.1. Presumed-PDF

In the presumed-PDF method (the conventional FGM method), based on assumptions (b) and (c) in

Please cite this article as: A. Hadadpour, S. Xu, Y. Zhang et al., An extended FGM model with transported PDF for LES of spray combustion, Proceedings of the Combustion Institute, https://doi.org/10.1016/j.proci.2022.09.014

Section 1, the joint-PDF is written as $\widetilde{P}(Z,\mathcal{C}) = \widetilde{P}(Z)\,\widetilde{P}(\mathcal{C})$ with presuming beta and delta distributions for the mixture fraction and progress variable [11], i.e., $\tilde{P}(Z) = \beta(Z;\tilde{Z},\widetilde{Z''^2})$ and $\tilde{P}(\mathcal{C}) = \delta(\mathcal{C}-\widetilde{\mathcal{C}})$. The values of $\tilde{Z}$ and $\widetilde{\mathcal{C}}$ are obtained from the corresponding transport equations; and the SGS mixture fraction variance ($\widetilde{Z''^2}$) is, typically, estimated using an algebraic model [11], $\widetilde{Z''^2} = C\Delta^2|\partial\tilde{Z}/\partial x_i|^2$, where C is model coefficient and Δ denotes the LES filter width. With these simplifications, $\widetilde{\psi}_\alpha$ can be calculated under the conditions that the assumptions are valid.

2.2.2. Transported-PDF

Alternatively, a TPDF approach based on the ESF method is proposed. In this method, stochastic partial differential equations (SPDEs) of Z, $\mathcal{Y}$ and sensible enthalpy h are solved. The unresolved scale fluctuations and the joint-PDF are represented by N_{esf} number of Eulerian stochastic fields. These SPDEs for the n^{th} ESF are written as:

$$\begin{aligned}\overline{\rho}d\xi_\alpha^{(n)} = &-\overline{\rho}\tilde{u}_i\frac{\partial\xi_\alpha^{(n)}}{\partial x_i}dt + \frac{\partial}{\partial x_i}(\Gamma_t\frac{\partial\xi_\alpha^{(n)}}{\partial x_i})dt\\ &+\overline{\rho}\sqrt{2\frac{\Gamma_t}{\overline{\rho}}}\frac{\partial\xi_\alpha^{(n)}}{\partial x_i}d\boldsymbol{W}_i^{(n)}\\ &-\frac{1}{2}\overline{\rho}C_\phi(\xi_\alpha^{(n)}-\tilde{\psi}_\alpha)\omega^{sgs}dt\\ &+\overline{\rho}S_\alpha^{r(n)}dt + \overline{S_\alpha^p}dt + \overline{S_\alpha^s}dt,\end{aligned} \tag{4}$$

with n=1,2,...,N_{esf}. Here, ξ_α represents Z, $\mathcal{Y}$ and h when $\alpha = 1, 2, 3$. $\tilde{\psi}_\alpha$ is the ensemble average of $\xi_\alpha^{(n)}$, i.e., Eq. 5. Γ_t is the sum of molecular and SGS diffusivity. The term $d\boldsymbol{W}_i^{(n)}$ represents a vector Wiener process that is spatially uniform but different for each field. Here, $d\boldsymbol{W}_i^{(n)}$ is approximated by time-step increment $\sqrt{dt}\eta^{(n)}$ and $\eta^{(n)}$ is a $\{-1, 1\}$ dichotomic random vector [5].

$\overline{S_\alpha^s}$ is spray source term in Z, $\mathcal{Y}$ and h equations. $\overline{S_\alpha^p}$ is the source term from pressure (p) change, which is only valid for sensible enthalpy equation, i.e., $\overline{S_\alpha^p} = \partial p/\partial t$ when $\alpha = 3$. $S_\alpha^{r(n)}$ is reaction source term interpolated from FGM tables. Note that, the reaction source terms are not filtered and are in closed form. Therefore, they can be directly computed from the FGM tables. Thus, no integration using a presumed PDF (Eq. 3) is needed. The filtered thermochemical properties are, then, calculated from the ensemble of N_{esf} notional fields, e.g.,

$$\widetilde{\psi}_\alpha = \frac{1}{N_{esf}}\sum_{n=1}^{N_{esf}}\xi_\alpha^{(n)}. \tag{5}$$

This equation is used for calculation of the fields $\widetilde{Z}$, $\widetilde{\mathcal{Y}}$, and $\widetilde{h}$.

The term involves C_ϕ is micro-mixing term and it is modelled using the Interaction by Exchange with the Mean (IEM) model [12]. In the micro-mixing term, ω^{sgs} is SGS turbulent frequency modeled as $\omega^{sgs} = (\mu+\mu_{sgs})/\overline{\rho}\Delta^2$, with μ being the laminar viscosity and μ_{sgs} the SGS eddy viscosity.

2.3. Liquid-phase spray modelling

Closures for spray source terms are obtained by simulation of the liquid phase using an LPT method, in which the first and secondary breakups are modelled using the Rosin-Rammler distribution [13] and the Kelvin-Helmholtz Rayleigh-Taylor (KHRT) model [14]. The Spalding formula is implemented to calculate the droplet evaporation rate [15]. The Ranz-Marshall correlation is used to model heat transfer between the liquid and gas phases [16,17]. The LPT model interacts with the ensemble average of stochastic fields. Since, in the ESF method, each stochastic field is not a physical realization of the random variables [5] (e.g., temperature), the spray evaporation process does not interact with the temperature in a single ESF [18,19]. Improved modelling of the spray process, however, is achieved when the local/temporal gas-phase thermodynamic state at each point/time is recast by ensemble averaging the stochastic fields. Additionally, the effects of unresolved SGS fluctuations on the LPT particles are considered through the stochastic turbulence dispersion [20].

In the FGM modelling of spray combustion, cooling effects of liquid fuel evaporation must be taken into account for the calculation of temperature (T). To perform this calculation, an approach, which is discussed and validated in Ref. [11], is adopted. In this approach, the transport equation for sensible enthalpy, h, is solved separately in the simulations. The temperature is then evaluated based on the calculated enthalpy and mass fraction of species. Since the h equation includes a spray source term, the energy exchange between the liquid and the gas phase, hence, the associated cooling effects of spray evaporation are taken into account in the calculation of temperature. The evaporation mainly affects the temperature in the liquid spray region, and its effect is expected to be milder downstream of this region where the ignition and majority of reactions take place. Although this effect on the species mass fraction could also be modeled by varying fuel-side temperature in the FGM tables at the cost of adding an additional table entry, Ref. [11] demonstrated that the final results in the case of this study are almost insensitive to such change of the fuel-side temperature.

2.4. Solution procedure

The solution procedure at each time step for the ESF/FGM method is summarized as follows: (1)

Please cite this article as: A. Hadadpour, S. Xu, Y. Zhang et al., An extended FGM model with transported PDF for LES of spray combustion, Proceedings of the Combustion Institute, https://doi.org/10.1016/j.proci.2022.09.014

Conservation equations of mass and momentum along with the ESF equations of mixture fraction, reaction progress variable and enthalpy (Eqs. 1, 2 and 4, respectively) are solved numerically using the conventional finite volume method. (2) The reaction source terms, $S_{\mathcal{Y}}^{r(n)}$ and $S_h^{r(n)}$ in Eq. 4, as well as $Y_i^{(n)}$ are obtained from the pre-generated FGM tables, using $Z^{(n)}$ and $\mathcal{C}^{(n)}$ as table entries. (3) The temperature, density and other thermodynamic properties of each ESF are calculated using $Y_i^{(n)}$ and $h^{(n)}$. (4) Finally, the mean values of species mass fractions, temperature, heat release rate (HRR), mixture fraction and other variables are calculated using its stochastic fields.

The method is implemented in OpenFOAM [21], and the solution procedure includes momentum predictor, pressure solver and the momentum corrector, sequentially. Second-order discretization schemes for both time and space are employed. The FGM table is generated by solving flamelet equations for counterflow diffusion flames in mixture fraction space, using the software FlameMaster [22].

3. Case specification and FGM tables

The Spray-A case from Engine Combustion Network (ECN), which is designed to mimic spray combustion in engines, is simulated. This case has been widely studied experimentally and numerically [23–25] and valuable measurements are available for the performance assessment of the new method. In the Spray-A case, 3.46 mg of n-dodecane fuel at 363 K is injected through a nozzle with a diameter of 90 μm into a constant-volume cubic vessel with a side length of 108 mm. The injection pressure and duration are 150 MPa and 1.5 ms, respectively. The temperature and density of the vessel prior to the injection of liquid n-dodecane are 900 K and 22.8 kg/m^3. The volumetric fractions of O_2, CO_2, H_2O and N_2 are 15%, 6.22%, 3.62% and 75.16%, respectively, in the reacting cases. These values mimic diesel engines with moderate exhaust gas recirculation (EGR). A non-reacting case is also simulated and used for spray modelling validation. The initial volumetric fractions of O_2, CO_2, H_2O and N_2 for the non-reacting case are 0%, 6.52%, 3.77% and 89.71%, respectively [26].

For reacting cases, the FGM method requires a pre-generated manifold, which consists of both unsteady and steady-state solutions of flamelet equations [4]. In the current work, a chemical kinetic mechanism, which consists of 130 species and 2323 reactions [27], is used. A set of one-dimensional flamelet equations is solved, first, to examine the scalar dissipation rates. The $\chi = 30$ s^{-1}, which is the scalar dissipation rate at the stoichiometric mixture fraction, is chosen for the unsteady flamelets as it well-predicts the reported n-dodecane IDT [26]. 429 unsteady solutions with $\chi = 30$ s^{-1}, and 47 steady-state solutions of the flamelet equation with χ ranging from 2×10^{-5} s^{-1} to 30 s^{-1}, are then used for the FGM database generation. To unify the unsteady and steady databases, a reaction progress variable, $\mathcal{Y}$, is needed. For any given Z, the chosen $\mathcal{Y}$ must increase monotonically alongside the reaction progress for unsteady flamelets and continue to increase monotonically as a function of χ for steady flamelets. In the following, we define two reaction progress variables ($\mathcal{Y}_{1,2}$) and examine their monotonicity and performance.

Table 1
Specification of the numerical cases.

	TCI	N_{esf}	$\mathcal{Y}$
Case 1 (baseline)	ESF	8	$\mathcal{Y}_2$
Case 2	ESF	4	$\mathcal{Y}_2$
Case 3	ESF	16	$\mathcal{Y}_2$
Case 4	ESF	32	$\mathcal{Y}_2$
Case 5	ESF	64	$\mathcal{Y}_2$
Case 6	ESF	128	$\mathcal{Y}_2$
Case 7	Presumed-PDF	-	$\mathcal{Y}_2$
Case 8	ESF	8	$\mathcal{Y}_1$

The first progress variable, $\mathcal{Y}_1$, is adopted from an often-used definition in similar FGM studies [11,24], $\mathcal{Y}_1 = Y^*_{CO}/M_{CO} + Y^*_{CH_2O}/M_{CH_2O} + Y^*_{CO_2}/M_{CO_2}$. Herein, M_i is the molecular mass of species and $Y_i^* = Y_i - Y_{N_2}(Y_i^0/Y_{N_2}^0)$, where superscript 0 denotes the initial value. The term $Y_{N_2}(Y_i^0/Y_{N_2}^0)$ estimates the local contribution of initial gases to Y_i, and it is thus used to exclude the contribution of the initial EGR gases to the reaction progress. Therefore, Y^* represents the local value of the species that is formed or consumed as a result of the reaction. This estimation is based on an assumption that the diffusion coefficients of all species are the same; thus, the local contribution of the initial mixture is proportional to the mass fraction of N_2, which is an inert gas in the current simulation.

The second progress variable, $\mathcal{Y}_2$, which is proposed in this work and is used as baseline progress variable, is $\mathcal{Y}_2 = Y_{N_2}(Y_{O_2}^0/Y_{N_2}^0) - Y_{O_2}$. Term $Y_{N_2}(Y_{O_2}^0/Y_{N_2}^0)$ estimates the amount of local oxygen in case of no reaction; and Y_{O_2} is the actual local mass fraction of oxygen. Therefore, their difference indicates how much oxygen has been locally consumed, hence, how much progress has been made in the reaction. The advantages of using $\mathcal{Y}_2$ and its limitations will be discussed in Section 4.2.

Table 1 shows the specification of the numerical cases. Case 1 employs 8 ESF and $\mathcal{Y}_2$ as progress variable. Cases 2–6 with 4–128 ESF are simulated to examine the sensitivity of the results and the shape of joint-PDF to the number of ESF. Case 7 with presumed-PDF is also simulated for comparison of ESF/FGM results with the conven-

Please cite this article as: A. Hadadpour, S. Xu, Y. Zhang et al., An extended FGM model with transported PDF for LES of spray combustion, Proceedings of the Combustion Institute, https://doi.org/10.1016/j.proci.2022.09.014

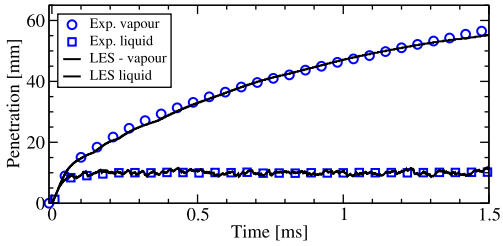

Fig. 1. Liquid and vapor penetration lengths of the non-reacting spray case from LES and experiment [26].

tional FGM results. Case 8 is defined to put into perspective the performance of the new progress variable in comparison with $\mathcal{Y}_1$.

The LES mesh size is 125 μm within the first 20 mm of the injector in the axial direction (spray region) and then it is increased to 250 μm for the rest of the flame region. A time step of Δt =20 ns is used, which keeps the maximum Courant number below 0.1. In addition to the analysis of mesh size in our previous works [20,28], the sufficiency of the used mesh in resolving the required fraction of turbulence is examined by applying three mesh grids, including a coarser mesh, the baseline mesh and a finer mesh with the total cell number of 0.44, 1.67, and 11.39 million, respectively. The grid sensitivity study (shown in Section 4.1, Fig. 3) shows that the baseline LES mesh and filter size (cubic root of the cell volume) are sufficient to well predict the pressure rise, ignition delay time (IDT) and flame lift-off length (LOL).

4. Results and discussion

The spray model is first examined by simulation of the non-reacting case, and the LPT setup is validated against the experimental measurements. Fig. 1 shows the calculated liquid and vapour penetration lengths, which agree well with the experiment [26]. Following the ECN recommendation [26], here the mixture fraction of 0.001 is considered as a threshold for the calculation of vapor penetration. The liquid length is calculated by considering the shortest axial distance from the injector in which 95% of liquid exists. The non-reacting results show that the current LES LPT model predicts well the liquid and vapor penetration lengths measured in the ECN experiment.

The validated spray setup is then applied for spray flame simulations and the results are presented in the following. In Fig. 2, the structure of the simulated spray flame of the baseline case using ESF/FGM is compared with the experiment. The left snapshots in this figure show the experimental hydroxyl (OH) radical chemiluminescence and the soot luminosity, and the blue line identifies the high-temperature region boundary [26,29].

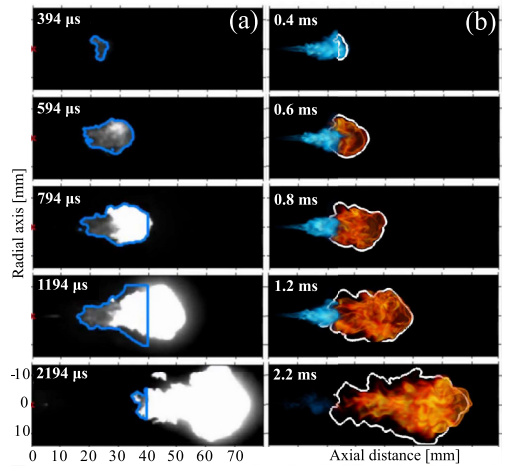

Fig. 2. The structure of transient spray flames. (a) Combustion chemiluminescence and soot luminosity in experiments [26,29]. The blue line is the measured high-temperature reactivity border. (b) Line-of-sight distribution of CH_2O (blue) and OH (yellow/red) predicted in the LES baseline case. The white line is isocontour of T=1100 K. (For interpretation of the references to colour in this figure legend, the reader is referred to the web version of this article.)

The right snapshots show the current simulation results of the line-of-sight distribution of formaldehyde (CH_2O) and OH, as well as the isocontour of T=1100 K (white line). The first igniting site in the simulations is observed around t=0.4 ms, as highlighted in Fig. 2, at the same location observed in the experiment. Following the onset of ignition, the high-temperature region develops both radially and axially, similar to that in the experiment. The simulation results agree reasonably well with experiments during the quasi-steady-state period of the injection, e.g., at 0.8 ms and 1.2 ms, and also after the end of injection, e.g., at t=2.2 ms, which is 0.7 ms after the end of injection.

4.1. ESF/FGM Results vs. conventional FGM results

The LES-predicted pressure rise is compared with the measurements in Fig. 3a. The dashed blue line represents transported-PDF cases with progress variable of $\mathcal{Y}_1$, i.e., Case 8 in Table 1. In the rest of the cases, $\mathcal{Y}_2$ is used. As can be seen, the results from $\mathcal{Y}_2$ agree reasonably well with the measurement, while the pressure rise from $\mathcal{Y}_1$ is under-predicted. Furthermore, as can be seen in this figure, the results of the ESF/FGM simulations with varying numbers of ESF agree well with experimental measurement and show low sensitivity to the number of ESF. The presumed-PDF model over-predicts the pressure rise as compared with the ESF model and the experiments. Underlying

Please cite this article as: A. Hadadpour, S. Xu, Y. Zhang et al., An extended FGM model with transported PDF for LES of spray combustion, Proceedings of the Combustion Institute, https://doi.org/10.1016/j.proci.2022.09.014

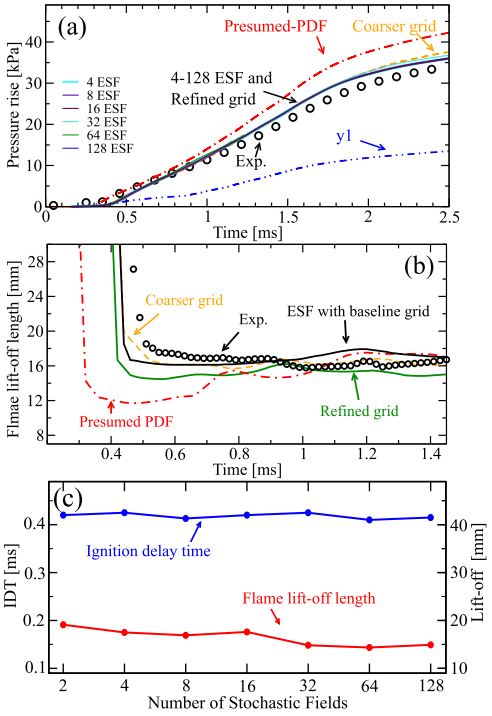

Fig. 3. (a) The pressure rise in experimental measurements and in different LES cases using $\mathcal{Y}_1$, and $\mathcal{Y}_2$ with presumed-PDF and transported-PDF, and the baseline, coarser and refined grids. The pressure rise profiles obtained with 4–128 ESF are almost identical. (b) Temporal evolution of instantaneous LOL. (c) LES-predicted LOL and IDT, with different N_{esf}.

reasons for the observed improvements in the results using $\mathcal{Y}_2$ and ESF/FGM will be discussed in the following section.

The instantaneous LOL from presumed-PDF and the ESF/FGM results are shown and compared with experiments in Fig. 3b. LOL is defined according to ECN recommendations [26], as the first axial location of OH mass fraction reaching 2% of its maximum in the domain. As can be seen, after the onset of ignition, the flame propagates toward the injector and reaches its quasi-steady lift-off location, and then it starts to oscillate. While both simulations predict a generally acceptable LOL, the ESF/FGM exhibits a more similar evolution to the experiment.

Fig. 3 c shows the time-averaged LOL and IDT values from cases with different numbers of ESF. The IDT is defined as the time after the start of injection when the maximum time-derivative of the temperature maximum occurs [26]. Results show that the values of LOL and IDT in this method are not greatly sensitive to the number of ESF. Additionally, the predicted LOL and IDT in the baseline case with ESF/FGM, i.e., 16.9 mm and 0.41 ms,

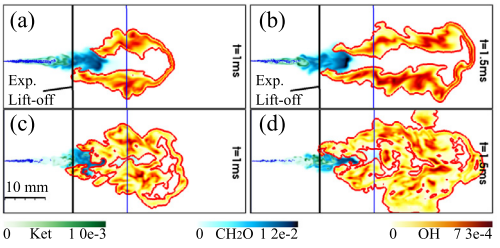

Fig. 4. (a) and (b) ESF/FGM simulation results at t=1 ms and 1.5 ms, respectively; (c) and (d) presumed-PDF/FGM simulation results at t=1 ms and 1.5 ms, respectively. The snapshots show mass fraction distributions of keto-hydoperoxide (green), formaldehyde Y_{CH_2O} (blue), and hydroxyl Y_{OH} (yellow/red). The parcels of LPT droplets are also shown with blue dots. The red lines are the iso-contours of $Y_{OH} = 1.5 \times 10^{-5}$. The black lines indicate the location of the reported LOL in the experiment [26]. The blue lines indicate the axial location which is used in the plots in Fig. 5. (For interpretation of the references to colour in this figure legend, the reader is referred to the web version of this article.)

respectively, agree well with the experimental measurement, i.e., 16.5 mm and 0.43 ms. Furthermore, the presumed-PDF/FGM model predicts a slightly shorter LOL (15.5 mm) and IDT (0.35 ms).

In addition to the baseline grid, the simulation results with the coarser and refined grids are shown in Figs. 3a and b. As can be seen, the pressure rise and LOL are not greatly sensitive to the grid resolution. The time-averaged LOL values using the coarser, baseline and refined grids are 15.2 mm, 16.9 mm and 16.3 mm, and the calculated IDT using these grids are 0.38 ms, 0.41 ms and 0.40 ms, respectively.

The accurate prediction of the thermochemical structure of the spray flame, including the distribution of species, plays an important role in the correct prediction of emissions in modern engine simulations. In Fig. 4, we compare the distribution of species from ESF/FGM results (Figs. 4a and b) and those from conventional FGM results (Figs. 4c and d). These figures show the local distribution of OH, CH_2O and keto-hydroperoxide mass fractions on a 2D spray axis cross-section, at t=1 ms and 1.5 ms. As can be seen, the predicted distributions of species are substantially different. To confirm this observation quantitatively, the radial profiles of the mean OH mass fraction and its standard deviation at the axial location of 30 mm (indicated by blue lines in Fig. 4) from the injector are shown in Fig. 5. The values in Fig. 5 are time-averaged in a period of 1 ms to 1.5 ms and are also azimuthal averaged. As can be seen in Figs. 4 and 5, the ESF/FGM predictions show that OH radicals are concentrated in the surrounding of the flame, in a layer with ~6 mm thickness. However, in the conventional FGM results, the OH radicals are more scattered and a considerable amount of

Please cite this article as: A. Hadadpour, S. Xu, Y. Zhang et al., An extended FGM model with transported PDF for LES of spray combustion, Proceedings of the Combustion Institute, https://doi.org/10.1016/j.proci.2022.09.014

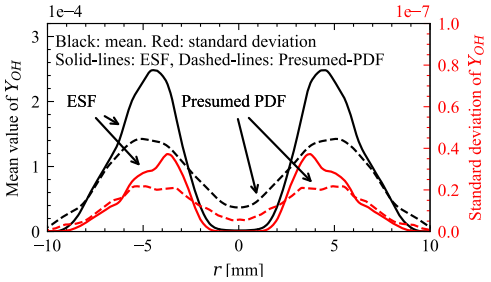

Fig. 5. The mean and standard deviation radial profiles of mass fraction of OH from ESF/FGM and presumed-PDF/FGM simulation results. The mean and deviation values are calculated in a period of 1 ms to 1.5 ms. The corresponding axial location used for this analysis (30 mm from the injector) is shown in Fig. 4 with a blue line. (For interpretation of the references to colour in this figure legend, the reader is referred to the web version of this article.)

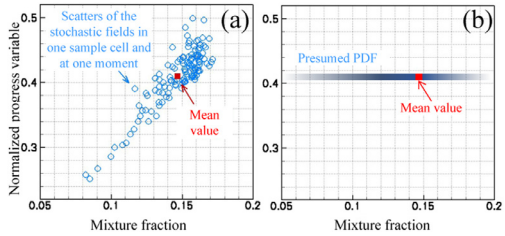

Fig. 6. Schematic illustration of the $Z - \mathcal{C}$ joint-PDF distributions in the ESF/FGM and presumed-PDF/FGM simulations. (a) The scatter of 128 ESF values of Z and $\mathcal{C}$ at t= 1 ms in one computational cell (on centerline at the axial location of 20 mm from the injector). (b) Schematic illustration of the typical joint-PDF in the presumed-PDF/FGM method. The red dot represents the mean (ensemble average) values of Z and $\mathcal{C}$ and the blue color indicates the PDF distribution. (For interpretation of the references to colour in this figure legend, the reader is referred to the web version of this article.)

these radicals can be seen in the core of flame, e.g., at r=0 mm, where r is the radial coordinate. This observation in the ESF/FGM results is in line with the experimental work in Ref. [30]. In that work, the flame structure in Spray-A was investigated using OH planar laser-induced fluorescence (PLIF). The PLIF measurement indicated that OH radicals are concentrated in a thin layer surrounding the rich mixture of the flame, which is well-captured in the present ESF/FGM simulations. It is worth mentioning that in the two simulations in the current work, an identical FGM database, identical mesh grid and identical spray setup are used, and the only difference is the representation of the SGS PDF. This shows that an improvement of the SGS PDF model can significantly improve the simulation of the reaction zone structures.

To understand underlying reasons for the observed differences in the results, the representation of SGS variations in the conventional FGM and ESF/FGM methods must be investigated. In the ESF/FGM method, the SGS variations are calculated from a set of stochastic fields. The fluctuations of unresolved scales are taken into account via the Wiener terms in the corresponding transport equations (Eq. 4). Fig. 6a, as an example, shows the resulting scatter of Z and $\mathcal{C}$ stochastic fields at one instant of time (t= 1 ms) and one computational cell (on the centerline, at 20 mm from the injector) for the case with 128 ESF. On the contrary, in the conventional FGM method, SGS variations are modelled by presuming a PDF for Z and $\mathcal{C}$ (typically beta-function for Z and delta-function for $\mathcal{C}$), as schematically shown in Fig. 6b. In the use of delta-function distribution in the presumed-PDF/FGM method, it is assumed that there is no scatter of progress variable along the vertical axis in Fig. 6.

To further investigate the joint-PDF of Z and $\mathcal{C}$ in the ESF results, a sampling of the ESF of these quantities is performed at three locations for a period of t=0.5 ms to 1 ms, with a rate of 50,000 samples per ms. These locations are along the centerline with the axial position of (I) 15 mm, (II) 20 mm and (III) 25 mm, and are chosen to represent, respectively, the low-temperature chemistry region, the fuel-rich premixed flame front, and the post oxidation zone, following the Dec's conceptual model [31]. The results of the calculated joint-PDF are shown in Fig. 7 for Case 6 and Case 1. It can be seen that the joint-PDF of Z and $\mathcal{C}$ does not exhibit a statistically independent behaviour. This can be understood by comparing the distribution of Z, for instance, at $\mathcal{C}$=0.2 with that at $\mathcal{C}$=0.5. This statistically dependence is in contradiction to the assumption (b) in the conventional FGM method (see Section 1). Additionally, the results show that the delta-function distribution which is typically used as a presumed-PDF distribution for the progress variable, i.e., assumption (c), can be invalid. Therefore, despite the use of the same FGM database in both presumed-PDF/FGM and ESF/FGM simulations, the joint-PDF of Z and $\mathcal{C}$ from these two methods is substantially different, which gives rise to the different flame structures in Fig. 4.

In the joint-PDFs, shown in Fig. 7, one can see a correlation between Z and $\mathcal{C}$ in the different regions of the flame. In the low-temperature ignition zone, i.e., point I, the increase of the progress variable takes place at rich mixtures ($Z > 0.1$), with the highest progress variable value in the vicinity of Z=0.2. In the fuel-rich premixed flame front (point II), however, the highest progress variable values are shifting towards the stoichiometric mixture. In the post oxidation zone, i.e., point III, the PDF distribution indicates that the majority of the mixture is approaching the maximum progress variable values, while a tail of low progress variable can be observed. This tail has

Please cite this article as: A. Hadadpour, S. Xu, Y. Zhang et al., An extended FGM model with transported PDF for LES of spray combustion, Proceedings of the Combustion Institute, https://doi.org/10.1016/j.proci.2022.09.014

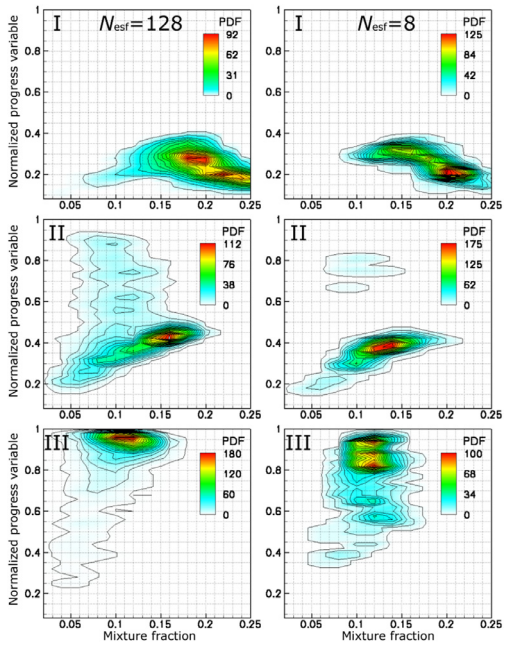

Fig. 7. The shape of joint-PDF of Z (mixture fraction) and $\mathcal{C}$ (normalized reaction progress variable) from the ESF/FGM simulations with 128 (left) and 8 ESF (right) on three sample points I, II, and III, which correspond to centerline positions at 15, 20 and 25 mm downstream the injector, respectively. Note that the maximum value of PDF depends on the shape and spread of the PDF.

a rather low PDF and it indicates ongoing reactions downstream of the fuel-rich premixed flame. In these figures, one can see that the joint-PDF from 8 ESF is generally similar to that from 128 ESF. Despite some local differences, the 8 numbers of ESF can resemble the main characteristics of the results with 128 ESF. This observation explains the similarities between the results with the varying number of fields and supports the discussions in Section 4.1 on minor sensitivity of results to N_{esf}. This is in line with the literature [32] and confirms the sufficiency of low numbers of ESF for spray flame simulations. Additionally, it should be noted that in LES, the differences between stochastic fields represent the sub-grid variance, which is much smaller than that in RANS simulations [33].

4.2. The new reaction progress variable

To investigate further the results in Fig. 3a, the distribution of $\mathcal{Y}_{1,2}$ values for steady and unsteady flamelets as a function of mixture fraction are shown in Fig. 8. As can be seen for $\mathcal{Y}_1$, some of the flamelets, which are identified by dashed red lines, exhibit a non-monotonic behaviour and there are cross lines between the flamelets. The value of $\mathcal{Y}_1$ in these unsteady flamelets (red dashed lines) increases first and exceeds the steady-state values and then decreases. This is because the mass fractions of some of the intermediate species (i.e., CH_2O and CO) are added to the definition of $\mathcal{Y}_1$ to capture the pre-ignition and ignition periods. However, since these species are consumed during the post-ignition period, the value of $\mathcal{Y}_1$ decreases after ignition. Therefore, $\mathcal{Y}_1$ values violate the monotonicity criterion. As discussed in Section 1, to cope with this problem in the FGM tabulation, this red-marked non-monotonic part of the solution is usually eliminated (see Ref. [11]). Unlike $\mathcal{Y}_1$, $\mathcal{Y}_2$ increases monotonically over the entire range of FGM space, as can be seen in Fig. 8b. To explore the effect of elimination of some flamelets in $\mathcal{Y}_1$ tables, the tabulated HRR from the FGM database with $\mathcal{Y}_{1-2}$ is shown in Figs. 8c-d, respectively, as an example of the tabulated quantities. Substantial differences can be seen in $\mathcal{Y}_1$ table compared to $\mathcal{Y}_2$ table. This can be seen by considering the distribution of the HRR in the range of $0.4 < \mathcal{C}_1 < 1$. In this range, a considerable amount of post-ignition heat release in $\mathcal{Y}_2$ is missing in $\mathcal{Y}_1$, as a result of the elimination of non-monotonic flamelets. Consequently, the $\mathcal{Y}_1$-based FGM model cannot predict the post-ignition heat release correctly. Thus, the predicted pressure rise is lower than the experimental results as shown in Fig. 3a.

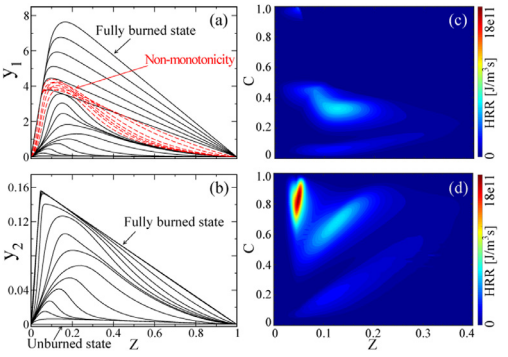

Fig. 8. The distribution of (a) $\mathcal{Y}_1$ and (b) $\mathcal{Y}_2$ from the steady and unsteady flamelet solutions. The red dashed lines show the non-monotonic part of the flamelets. Note that only a few samples of 476 flamelets used in this study are shown in these plots, to keep the lines visible and distinguishable. The right side figures show the tabulated HRR, as an example of tabulated quantities, in Z–$\mathcal{C}$ space, calculated from the FGM database with (c) $\mathcal{Y}_1$ and (d) $\mathcal{Y}_2$. (For interpretation of the references to colour in this figure legend, the reader is referred to the web version of this article.)

5. Conclusion

A novel ESF/FGM approach was formulated for modelling spray combustion in engine-like applications. Two of the key assumptions in the FGM

Please cite this article as: A. Hadadpour, S. Xu, Y. Zhang et al., An extended FGM model with transported PDF for LES of spray combustion, Proceedings of the Combustion Institute, https://doi.org/10.1016/j.proci.2022.09.014

method were removed in the new method and replaced by a transported-PDF approach, based on ESF. The performance of the new method was analyzed by performing LES for the ECN Spray-A n-dodecane combustion, under conditions relevant to internal combustion engines. It was shown that ESF/FGM is capable of replicating the experimental observations in terms of IDT, LOL, HRR and pressure rise, as well as the thermo-chemical structure of the flame.

It was discussed that the structure of spray flame in ESF/FGM simulation is substantially different from that in the conventional FGM simulation, while the global characteristics such as IDT, LOL and pressure rise from the two simulation approaches are only moderately different. It was also shown that in contrast to conventional flamelet assumptions, the represented SGS fluctuations of table-entry quantities (Z and $\mathcal{C}$) in ESF/FGM are not statistically independent.

Finally, two reaction progress variables were examined for the ESF/FGM simulations. The commonly used progress variables in literature failed to predict the later stages of combustion. The underlying reason for this observation was investigated and it was shown that the non-monotonic behaviour of such progress variable after ignition could lead to neglecting an important part of the reaction progress. Therefore, quantities such as pressure rise could not be predicted using this progress variable. A new progress variable was proposed based on the oxygen molecule consumption and its performance was examined and validated for Spray-A flame. The new progress variable does not require any ad hoc adjustment which makes it a good choice for many applications.

Declaration of Competing Interest

The authors declare that they have no known competing financial interests or personal relationships that could have appeared to influence the work reported in this paper.

Acknowledgments

This work was sponsored by the Swedish Research Council (VR). AH was partially sponsored by Scania CV AB. SX and YZ were partially sponsored by the China Scholarship Council (CSC). The simulations were performed on NSC, HPC2N and PDC provided by the Swedish National Infrastructure for Computing (SNIC).

References

[1] R.D. Reitz, Directions in internal combustion engine research, Combust. Flame. 160 (1) (2013) 1–8.
[2] C.D. Pierce, P. Moin, Progress-variable approach for large-eddy simulation of non-premixed turbulent combustion, J. Fluid. Mech. 504 (2004) 73–97.
[3] H. Pitsch, M. Ihme, An unsteady/flamelet progress variable method for LES of nonpremixed turbulent combustion, 43rd AIAA Aerospace Sci. Meet. Exhibit (2005) 557.
[4] J. Van Oijen, L. De Goey, Modelling of premixed laminar flames using flamelet-generated manifolds, Combust. Sci. Technol. 161 (1) (2000) 113–137.
[5] L. Valiño, A field monte carlo formulation for calculating the probability density function of a single scalar in a turbulent flow, Flow. Turbul. Combust. 60 (2) (1998) 157–172.
[6] D.C. Haworth, Progress in probability density function methods for turbulent reacting flows, Prog. Energ. Combust. 36 (2) (2010) 168–259.
[7] J. Kuehne, A. Ketelheun, J. Janicka, Analysis of sub-grid PDF of a progress variable approach using a hybrid LES/TPDF method, P. Combust. Inst. 33 (1) (2011) 1411–1418.
[8] A. Avdić, G. Kuenne, F. di Mare, J. Janicka, LES Combustion modeling using the eulerian stochastic field method coupled with tabulated chemistry, Combust. Flame. 175 (2017) 201–219.
[9] R. Mahmoud, M. Jangi, F. Ries, B. Fiorina, J. Janicka, A. Sadiki, Combustion characteristics of a non-Premixed oxy-Flame applying a hybrid filtered eulerian stochastic field/flamelet progress variable approach, Appl. Sci. 9 (7) (2019) 1320.
[10] M. Jangi, X. Zhao, D.C. Haworth, et al, Stabilization and liftoff length of a non-premixed methane/air jet flame discharging into a high-temperature environment: an accelerated transported PDF method, Combust. Flame. 162 (2) (2015) 408–419.
[11] A. Wehrfritz, O. Kaario, V. Vuorinen, B. Somers, Large eddy simulation of n-dodecane spray flames using flamelet generated manifolds, Combust. Flame. 167 (2016) 113–131.
[12] C. Dopazo, Relaxation of initial probability density functions in the turbulent convection of scalar fields, Phys. Fluids. 22 (1) (1979) 20–30.
[13] W.E. Ranz, Evaporation from drops, parts i & II, Chem. Eng. Prog. 48 (1952) 141–146.
[14] R. Reitz, Modeling atomization processes in high–pressure vaporizing sprays, Atomisat. Spray Tech. 3 (4) (1987) 309–337.
[15] D.B. Spalding, The combustion of liquid fuels, in: Symposium (International) on Combustion, volume 4, 1953, pp. 847–864.
[16] W.E. Ranz, W.R. Marshall, Evaporation from drops, part I, Chem. Eng. Prog. 48 (3) (1952) 141–146.
[17] W.E. Ranz, W.R. Marshall, Evaporation from drops, part II, Chem. Eng. Prog. 48 (3) (1952) 173–180.
[18] K.M. Pang, M. Jangi, X.-S. Bai, et al., Modelling of diesel spray flames under engine-like conditions using an accelerated eulerian stochastic field method, Combust. Flame. 193 (2018) 363–383.
[19] S. Xu, K.M. Pang, Y. Li, et al., LES/TPDF Investigation of the effects of ambient methanol concentration on pilot fuel ignition characteristics and reaction front structures, Fuel 287 (2021) 119502.
[20] M. Jangi, R. Solsjo, B. Johansson, X.-S. Bai, On large eddy simulation of diesel spray for internal combustion engines, Int. J. Heat. Fluid. Fl. 53 (2015) 68–80.

Please cite this article as: A. Hadadpour, S. Xu, Y. Zhang et al., An extended FGM model with transported PDF for LES of spray combustion, Proceedings of the Combustion Institute, https://doi.org/10.1016/j.proci.2022.09.014

[21] H. Jasak, A. Jemcov, Z. Tukovic, Openfoam: A C++ library for complex physics simulations, Int. Workshop Coupled Method. Numer. Dyn. 1000 (2007) 1–20.
[22] H. Pitsch, FlameMaster: A C++ computer program for 0D combustion and 1D laminar flame calculations, 1998, (????).
[23] S. Ramezani, E. Amani, M. Saffar-Avval, A combined rate-shaping-splitting injection strategy for regulating stratification characteristics of fuel sprays, Appl. Therm. Eng. (2021) 116544.
[24] H. Kahila, A. Wehrfritz, O. Kaario, et al, Large-eddy simulation on the influence of injection pressure in reacting spray a, Combust. Flame. 191 (2018) 142–159.
[25] A. Hadadpour, M. Jangi, K.M. Pang, X.S. Bai, The role of a split injection strategy in the mixture formation and combustion of diesel spray: a large-eddy simulation, Proc. Combust. Inst. 37 (2019) 4709–4716.
[26] Sandia National Laboratories, Engine combustion network, Laboratories (2022). https://ecn.sandia.gov
[27] E. Ranzi, A. Frassoldati, A. Stagni, et al, Reduced kinetic schemes of complex reaction systems: fossil and biomass-derived transportation fuels, Int. J. Chem. Kinet. 46 (9) (2014) 512–542.
[28] C. Gong, M. Jangi, X.-S. Bai, Large eddy simulation of n-dodecane spray combustion in a high pressure combustion vessel, App. Energ. 136 (2014) 373–381.
[29] P.M. Lillo, L.M. Pickett, H. Persson, et al, Diesel spray ignition detection and spatial/temporal correction, SAE Int. J. Eng. 5 (3) (2012) 1330–1346.
[30] N. Maes, M. Meijer, N. Dam, et al., Characterization of spray a flame structure for parametric variations in ecn constant-volume vessels using chemiluminescence and laser-induced fluorescence, Combust. Flame. 174 (2016) 138–151.
[31] J.E. Dec, A conceptual model of DL diesel combustion based on laser-sheet imaging, SAE Trans. (1997) 1319–1348.
[32] W. Jones, A. Marquis, V. Prasad, LES Of a turbulent premixed swirl burner using the eulerian stochastic field method, Combust. Flame. 159 (10) (2012) 3079–3095.
[33] S. Zhong, S. Xu, X.-S. Bai, et al., Large eddy simulation of n-heptane/syngas pilot ignition spray combustion: ignition process, liftoff evolution and pollutant emissions, Energy 233 (2021) 121080.

Please cite this article as: A. Hadadpour, S. Xu, Y. Zhang et al., An extended FGM model with transported PDF for LES of spray combustion, Proceedings of the Combustion Institute, https://doi.org/10.1016/j.proci.2022.09.014